Nonstandard Finite Difference Time Domain Algorithm for Berenger's Perfectly Matched Layer

Naoki Okada and James B. Cole

Graduate School of Systems and Information Engineering
University of Tsukuba, 1-1-1 Tennodai, Tsukuba, Ibaraki 305-8573, Japan
okada@cavelab.cs.tsukuba.ac.jp, cole@cs.tsukuba.ac.jp

***Abstract*—**The nonstandard (NS) finite difference time domain (FDTD) algorithm provides remarkably high accuracy on a coarse grid by optimizing to monochromatic wave propagation within each uniform region. But, an effective absorbing boundary condition (ABC) is also necessary to accurately calculate electromagnetic fields. Although Berenger's perfectly matched layer (PML) is a highly effective ABC, there is still no NS-formulation of it. In this paper, we develop a NS-version of the PML (NS-PML). We compare the NS-PML with other ABCs and demonstrate its excellent absorption.

***Index Terms*—**Nonstandard finite difference time domain (NS-FDTD) algorithm, nonstandard perfectly matched layer (NS-PML), stability.

I. INTRODUCTION

The nonstandard (NS) finite difference time domain (FDTD) algorithm provides high accuracy on a coarse grid by optimizing to monochromatic wave propagation [1, 2, 3]. Even for subwavelength structures the NS-FDTD algorithm has performed successfully [4], but an effective absorbing boundary condition (ABC) is also necessary to accurately calculate electromagnetic fields. The improved second-order Mur ABC and higher-order ABCs shows good absorption [5, 6], but reflection at corners of the numerical grid is high and it is sometimes unstable. Although Berenger's perfectly matched layer (PML) [7] is a highly effective ABC, there is no NS-formulation of it.

We develop a NS-FDTD algorithm for the conductive Maxwell's equations in Section II, a NS-version of the PML (NS-PML) in Section III, and its stability in Section IV. We compare the NS-PML with other ABCs and demonstrate its excellent absorption in Section V.

II. NONSTANDARD FDTD ALGORITHM FOR THE CONDUCTIVE MAXWELL'S EQUATIONS

In dispersion-less and linear-isotropic media, the conductive Maxwell's equations are given by

$$(\mu\partial_t + \sigma^*)\,\mathbf{H} = -\nabla\times\mathbf{E}, \tag{1a}$$

$$(\varepsilon\partial_t + \sigma)\,\mathbf{E} = \nabla\times\mathbf{H}, \tag{1b}$$

where $\partial_t = \partial/\partial t$, $\mathbf{H}$ is the magnetic field, $\mathbf{E}$ is the electric field, μ is the permeability, ε is the permittivity, σ is the electric conductivity, and σ^* is the magnetic conductivity. Applying $\nabla\times$ to both sides of (1) and using the vector identity,

$$\nabla\times\nabla\times\mathbf{V} = \nabla(\nabla\cdot\mathbf{V}) - \nabla^2\mathbf{V},\ \ (\mathbf{V}=\mathbf{H},\mathbf{E}), \tag{2}$$

we obtain an absorbing wave equation in a medium with zero charge density,

$$\left(\partial_t^2 - v^2\nabla^2 + 2(a+a^*)\,\partial_t + 4aa^*\right)\psi = 0, \tag{3}$$

where $v = 1/\sqrt{\mu\varepsilon}$, $a = \sigma/(2\varepsilon)$, and $a^* = \sigma^*/(2\mu)$. The forward and backward solutions are

$$\psi_0 = e^{-(a+a^*)t}e^{i(\mathbf{k}\cdot\mathbf{r}\pm\bar{\omega}t)}, \tag{4}$$

where $\mathbf{r} = (x, y, z)$, $\mathbf{k}$ is the wave vector, and

$$\bar{\omega} = \sqrt{\omega^2 - (a-a^*)^2}, \tag{5}$$

where ω is the angular frequency.

Using the conventional finite difference time domain (FDTD) algorithm for $t = n\Delta t$, $x, y, z = mh$ ($n, m =$ integer), (3) is discretized as follows,

$$\left(d_t^2 - \frac{v^2\Delta t^2}{h^2}\mathbf{d}^2 + (\alpha+\alpha^*)\,\bar{d}_t + 4\alpha\alpha^*\right)\psi = 0, \tag{6}$$

where $\alpha = a\Delta t$, $\alpha^* = a^*\Delta t$, $d_t f(t) = f(t + \Delta t/2) - f(t - \Delta t/2)$, $\bar{d}_t f(t) = f(t+\Delta t) - f(t - \Delta t)$, and $\mathbf{d} = (d_x, d_y, d_z)$ (d_x, d_y, d_z are defined analogously to d_t). Inserting the solution (4) into (6), we find

$$\left(d_t^2 - \frac{v^2\Delta t^2}{h^2}\mathbf{d}^2 + (\alpha+\alpha^*)\,\bar{d}_t + 4\alpha\alpha^*\right)\psi_0 \neq 0. \tag{7}$$

The right side of (7) does not vanish, because ψ_0 is not a solution of the difference equation (6).

We now seek a nonstandard (NS) finite difference (FD) model of (3) which has the same solution as (3). Replacing $\mathbf{d}^2$ with $\mathbf{d}_0^2$ and h with $s(k,h)$, we find a high accuracy spatial FD expression (see Appendix A),

$$\nabla^2\psi_0 \cong \frac{\mathbf{d}_0^2\psi_0}{s(k,h)^2}, \quad s(k,h) = \frac{2}{k}\sin\left(\frac{kh}{2}\right), \tag{8}$$

and require that

$$\left(d_t^2 - u^2\mathbf{d}_0^2 + (\beta+\beta^*)\,\bar{d}_t + 4\beta\beta^*\right)\psi_0 = 0. \tag{9}$$

This is an example of a NS-FDTD algorithm. Let us find u, β, β^* for which (9) is exactly satisfied. The temporal-spatial FD expressions give

$$d_t^2\psi_0 = 4\sinh^2\left(\frac{\alpha+\alpha^* \pm i\bar{\omega}\Delta t}{2}\right)\psi_0, \tag{10}$$

$$\bar{d}_t\psi_0 = -2\sinh\left(\alpha+\alpha^* \pm i\bar{\omega}\Delta t\right)\psi_0, \tag{11}$$

$$\mathbf{d}_0^2\psi_0 = -4\sin^2\left(kh/2\right)\psi_0. \tag{12}$$

Substituting (10)-(12) into (9) and requiring that the imaginary part vanishes, we find

$$\beta = \frac{\tanh\alpha}{1+\tanh\alpha\tanh\alpha^*}, \tag{13}$$

$$\beta^* = \frac{\tanh\alpha^*}{1+\tanh\alpha\tanh\alpha^*}. \tag{14}$$

Setting the real part to zero, we obtain

$$u^2 = \frac{\sinh^2\left[(\alpha+\alpha^*)/2\right] + \sin^2\left(\bar{\omega}/2\right)}{\cosh\left(\alpha+\alpha^*\right)\sin^2\left(kh/2\right)} - \frac{\beta\beta^*}{\sin^2\left(kh/2\right)}. \tag{15}$$

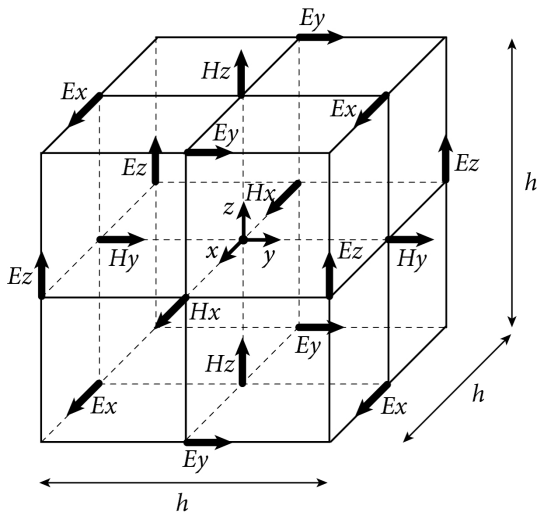

Fig. 1. Yee cell. h is the grid spacing. E_x, E_y, E_z are electric field components. H_x, H_y, H_z are magnetic field components. Components are staggered on the numerical grid.

From the NS-FDTD algorithm for the absorbing wave equation, we obtain the NS-FDTD algorithm for the conductive Maxwell's equations. According to [2], the NS-FDTD algorithm for the non-conductive Maxwell's equations is given by

$$d_t\mathbf{H} = -\frac{u_0}{Z}\mathbf{d}\times\mathbf{E}, \tag{16a}$$

$$d_t\mathbf{E} = u_0 Z\mathbf{d}_0\times\mathbf{H}, \tag{16b}$$

where $u_0 = \sin(\omega\Delta t/2)/\sin(kh/2)$, $Z = \sqrt{\mu/\varepsilon}$, and $\mathbf{d}_0 = \left(d_x^0, d_y^0, d_z^0\right)$ satisfies $\mathbf{d}\cdot\mathbf{d}_0 = \mathbf{d}_0\cdot\mathbf{d} = \mathbf{d}_0^2$ (see Appendix A). Following (16), we define

$$\left(d_t + 2\beta^*\right)\mathbf{H} = -\frac{u}{Z}\mathbf{d}\times\mathbf{E}, \tag{17a}$$

$$\left(d_t + 2\beta\right)\mathbf{E} = uZ\mathbf{d}_0\times\mathbf{H}. \tag{17b}$$

Using the discretized vector identity to which Gauss' law is applied,

$$\mathbf{d}_0\times\mathbf{d}\times\mathbf{V} = -\left(\mathbf{d}_0\cdot\mathbf{d}\right)\mathbf{V} = \mathbf{d}_0^2\mathbf{V}, \tag{18}$$

(17a) and (17b) can be transformed into (9). Thus, (17) is a NS-FDTD algorithm for the conductive Maxwell's equations optimized to monochromatic waves. As shown in Fig. 1, the electromagnetic field components are laid out on the grid,

$$\begin{cases} H_x(x+h/2, y, z, t-\Delta t/2), & \text{(19a)} \\ H_y(x, y+h/2, z, t-\Delta t/2), & \text{(19b)} \\ H_z(x, y, z+h/2, t-\Delta t/2), & \text{(19c)} \end{cases}$$

$$\begin{cases} E_x(x, y+h/2, z+h/2, t), & \text{(20a)} \\ E_y(x+h/2, y, z+h/2, t), & \text{(20b)} \\ E_z(x+h/2, y+h/2, z, t). & \text{(20c)} \end{cases}$$

Expanding the temporal finite difference operators, the NS-FDTD algorithm becomes

$$\mathbf{H}^{n+1/2} = \frac{\beta_-^*}{\beta_+^*}\mathbf{H}^{n-1/2} - \frac{u}{\beta_+^* Z}\mathbf{d}\times\mathbf{E}^n, \quad \text{(21a)}$$

$$\mathbf{E}^{n+1} = \frac{\beta_-}{\beta_+}\mathbf{E}^{n-1} + \frac{uZ}{\beta_+}\mathbf{d}_0\times\mathbf{H}^{n+1/2}, \quad \text{(21b)}$$

where $\beta_\pm = 1 \pm \beta$, $\beta_\pm^* = 1 \pm \beta^*$, and we simply write $\mathbf{H}(\mathbf{r}, t) \to \mathbf{H}^n$ (analogously for $\mathbf{E}$).

III. NONSTANDARD PERFECTLY MATCHED LAYER

We derive a nonstandard (NS) perfectly matched layer (PML) formulation based on Berenger's PML. According to the Berenger's PML, the conductive Maxwell's equations in the transverse magnetic (TM) mode ($\mathbf{E}$ parallel to media interfaces) are split by

$$\begin{aligned} \left(\mu\partial_t + \sigma_y^*\right) H_x &= -\partial_y E_z, & \text{(22a)} \\ \left(\mu\partial_t + \sigma_x^*\right) H_y &= \partial_x E_z, & \text{(22b)} \\ \left(\varepsilon\partial_t + \sigma_x\right) E_{zx} &= \partial_x H_y, & \text{(22c)} \\ \left(\varepsilon\partial_t + \sigma_y\right) E_{zy} &= -\partial_y H_x, & \text{(22d)} \end{aligned}$$

where $E_z = E_{zx} + E_{zy}$. The split Maxwell's equations are not equivalent to the absorbing wave equation in the PML, because Gauss' law is invalid for $\sigma_x \neq \sigma_y$. However, we found that the NS-FDTD algorithm based on the absorbing wave equation provides highly effective absorption even in the PML, as shown in Section V. Just as σ is separated into σ_x, σ_y in the PML, we separate $\beta(\sigma)$ into $\beta_x = \beta(\sigma_x)$, $\beta_y = \beta(\sigma_y)$ and $\beta^*(\sigma)$ into $\beta_x^* = \beta^*(\sigma_x)$, $\beta_y^* = \beta^*(\sigma_y)$ in (17). Thus, the NS-FDTD algorithm becomes

$$\begin{aligned} \left(d_t + 2\beta_y^*\right) H_x &= -\frac{u}{Z} d_y E_z, & \text{(23a)} \\ \left(d_t + 2\beta_x^*\right) H_y &= \frac{u}{Z} d_x E_z, & \text{(23b)} \\ \left(d_t + 2\beta_x\right) E_{zx} &= uZ d_x^0 H_y, & \text{(23c)} \\ \left(d_t + 2\beta_y\right) E_{zy} &= -uZ d_y^0 H_x, & \text{(23d)} \end{aligned}$$

where $u = u_0$ only inside the PML to promote the numerical stability as we discuss in Section IV. Expanding the temporal finite difference operators in the Yee cell, we obtain

$$\begin{aligned} H_x^{n+1/2} &= \frac{\beta_{y-}^*}{\beta_{y+}^*} H_x^{n-1/2} - \frac{u}{\beta_{y+}^* Z} d_y E_z^n, & \text{(24a)} \\ H_y^{n+1/2} &= \frac{\beta_{x-}^*}{\beta_{x+}^*} H_y^{n-1/2} + \frac{u}{\beta_{x+}^* Z} d_x E_z^n, & \text{(24b)} \\ E_{zx}^{n+1} &= \frac{\beta_{x-}}{\beta_{x+}} E_{zx}^{n-1} + \frac{uZ}{\beta_{x+}} d_x^0 H_y^{n+1/2}, & \text{(24c)} \\ E_{zy}^{n+1} &= \frac{\beta_{y-}}{\beta_{y+}} E_{zy}^{n-1} - \frac{uZ}{\beta_{y+}} d_y^0 H_x^{n+1/2}, & \text{(24d)} \end{aligned}$$

where $\beta_{i\pm} = 1 \pm \beta_i$, $\beta_{i\pm}^* = 1 \pm \beta_i^*$ $(i = x, y)$. In the transverse electric (TE) mode ($\mathbf{E}$ perpendicular to media interfaces), the conductive Maxwell's equations are split by

$$\begin{aligned} \left(\mu\partial_t + \sigma_x^*\right) H_{zx} &= -\partial_x E_y, & \text{(25a)} \\ \left(\mu\partial_t + \sigma_y^*\right) H_{zy} &= \partial_y E_x, & \text{(25b)} \\ \left(\varepsilon\partial_t + \sigma_y\right) E_x &= \partial_y H_z, & \text{(25c)} \\ \left(\varepsilon\partial_t + \sigma_x\right) E_y &= -\partial_x H_z, & \text{(25d)} \end{aligned}$$

where $H_z = H_{zx} + H_{zy}$. We separate β into β_x, β_y (analogously for β^*) and obtain

$$\begin{aligned} H_{zx}^{n+1/2} &= \frac{\beta_{x-}^*}{\beta_{x+}^*} H_{zx}^{n-1/2} - \frac{u}{\beta_{x+}^* Z} d_x E_z^n, & \text{(26a)} \\ H_{zy}^{n+1/2} &= \frac{\beta_{y-}^*}{\beta_{y+}^*} H_{zy}^{n-1/2} + \frac{u}{\beta_{y+}^* Z} d_y E_z^n, & \text{(26b)} \\ E_x^{n+1} &= \frac{\beta_{y-}}{\beta_{y+}} E_x^{n-1} + \frac{uZ}{\beta_{y+}} d_y^0 H_y^{n+1/2}, & \text{(26c)} \\ E_y^{n+1} &= \frac{\beta_{x-}}{\beta_{x+}} E_y^{n-1} - \frac{uZ}{\beta_{x+}} d_x^0 H_x^{n+1/2}, & \text{(26d)} \end{aligned}$$

where $u = u_0$ in the PML. In three dimensions, the NS-PML formulation is similarly derived using the separations based on Berenger's PML.

In two-dimensional PMLs, there is no reflection if the conductivities are continuous and the impedance matching condition is satisfied,

$$\sigma_x^*/\mu = \sigma_x/\varepsilon, \quad \sigma_y^*/\mu = \sigma_y/\varepsilon. \quad \text{(27)}$$

But there is a small reflection due to the discretization on a grid [8], the following definition gives a simple control of the absorption performance [9],

$$\sigma_x = \begin{cases} \sigma_m \left(1 - \frac{i}{L}\right)^M, & \text{for } i < L \quad \text{(28a)} \\ \sigma_m \left(1 - \frac{N-i}{L}\right)^M, & \text{for } i > N - L, \quad \text{(28b)} \end{cases}$$

$$\sigma_y = \begin{cases} \sigma_m \left(1 - \frac{j}{L}\right)^M, & \text{for } j < L \quad \text{(29a)} \\ \sigma_m \left(1 - \frac{N-j}{L}\right)^M, & \text{for } j > N - L, \quad \text{(29b)} \end{cases}$$

where $x = ih$, $y = jh$ $(i, j = 0, 1, \cdots, N)$, L is the number of PML layers, M is the damping constant, and σ_m is given by using the incidence angle θ and theoretical reflection coefficient R_{th},

$$\sigma_m = -\frac{(M+1)\varepsilon v}{2Lh\cos\theta}\ln R_{th}. \tag{30}$$

We empirically choose $\theta = 60°$, $R_{th} = 10^{-8}$, and $M = 2$.

IV. NUMERICAL STABILITY

The numerical stability of the NS-FDTD algorithm for the conductive Maxwell's equations is the same as the absorbing wave equation, because they are equivalent in homogeneous media as shown in Section II. Thus, we derive the stability for latter. For a monochromatic wave, we obtain

$$\mathbf{d}_0^2\psi_0 = -D^2\psi_0, \tag{31}$$

where D^2 is given later. Using (31), the NS-FDTD algorithm (9) is rewritten in the form,

$$\begin{pmatrix} \psi_0^n \\ \psi_0^{n+1} \end{pmatrix} = A^n \begin{pmatrix} \psi_0^0 \\ \psi_0^1 \end{pmatrix}, \tag{32}$$

where we simply write $\psi_0(\mathbf{r}, n\Delta t) \to \psi_0^n$, and

$$A = \begin{pmatrix} 0 & 1 \\ -\frac{1-\beta-\beta^*}{1+\beta+\beta^*} & \frac{2-4\beta\beta^*-u^2D^2}{1+\beta+\beta^*} \end{pmatrix}. \tag{33}$$

Since the eigenvalue of A gives the algorithm stability (see Appendix B), we find

$$u^2 \le \frac{2 - 4\beta\beta^* + 2\sqrt{1-(\beta+\beta^*)^2}}{D^2}. \tag{34}$$

The strictest condition on u^2 is found by taking the maximum possible value of D^2 in (34). Solving $\partial_{k_p} D^2 = 0$ $(p = x, y, z)$ in each dimension, we obtain

$$\max\left(D^2\right) = \begin{cases} 4, & \text{for 1-D} \quad (35a) \\ \dfrac{1}{\gamma_1}, & \text{for 2-D} \quad (35b) \\ \dfrac{\gamma_1}{\gamma_2}\left(3 - \dfrac{2\gamma_1^2}{\gamma_2}\right), & \text{for 3-D,} \quad (35c) \end{cases}$$

where γ_1 and γ_2 are defined in Appendix A. Although the stability is almost-completely satisfied in the PML because electromagnetic waves are exponentially damped, non-physical separated conductivities sometimes cause instability [10, 11]. Thus, we replace conductivity-dependent u with conductivity-independent u_0 in the PML.

Table 1: Example simulation parameters

medium	vacuum
wavelength	500 nm
grid spacing	50 nm
beam width	15μm
computational domain	120μm $\times$ 60μm

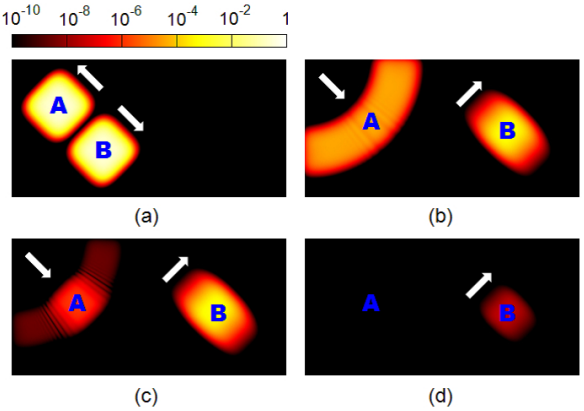

Fig. 2. Comparison of nonstandard (NS) absorbing boundary conditions (ABCs). White arrows show propagation directions of pulses. (a) Incident pulses: A is incident on a corner of the computational domain, while B is incident on a side. Reflections of pulses A and B with (b) NS-Mur ABC, (c) NS-Higdon ABC, and (d) $L = 8$ layer NS-PML.

V. PERFORMANCE VALIDATION

We compare the NS-PML with the nonstandard Mur (NS-Mur) [5] and Higdon (NS-Higdon) absorbing boundary conditions (ABCs). Similarly to the NS-Mur ABC, the NS-Higdon ABC is simply derived from the conventional Higdon ABC [12] by replacing $v\Delta t/h$ with u_0.

Using the example parameters listed in Table 1, we simulate absorptions at an optical wavelength on a coarse grid in the TM mode. Figure 2 shows intensity distributions of reflections using the NS-Mur, NS-Higdon, and NS-PML of $L = 8$ layers. Figure 2(a) shows incident pulses impinge upon the boundary at an angle of $\theta = 45°$ from the normal (A is incident on a corner of the computational domain, B is incident on a side). In Fig. 2(b),

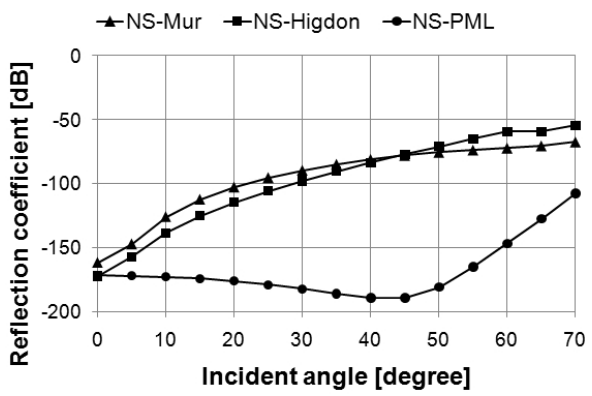

Fig. 3. Angular reflection spectrum of NS-PML ($L = 8$ layers) compared with NS-Mur and NS-Higdon.

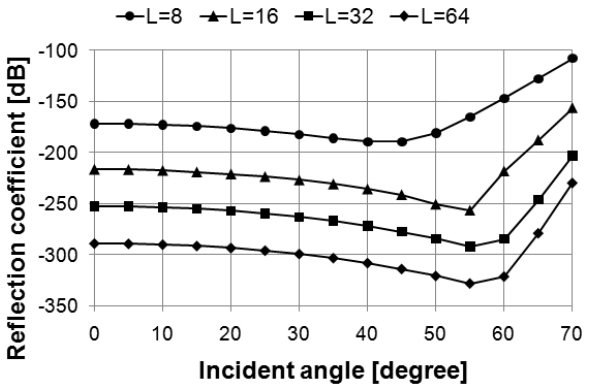

Fig. 4. Angular reflection spectrum of NS-PML with different numbers of layers, $L = 8$, 16, 32, and 64.

the NS-Mur generates large reflections for pulse A (about -80 dB) because corner values are approximated. In Fig. 2(c), the NS-Higdon improves the corner absorption, but it also has about the same reflection as the NS-Mur for pulse B. Whereas, in Fig. 2(d), the NS-PML of 8 layers greatly reduces the reflections for both pulses (about -190 dB).

Using the parameters of Table 1, we calculate the reflection coefficient, which is defined by the ratio of pulse B intensities before and after reflection on a side. In Fig. 3, we show the angular reflection spectra using the NS-Mur, NS-Higdon, and NS-PML of $L = 8$ layers. For both the NS-Mur and NS-Higdon, the reflection rapidly increases with incidence angle, whereas the NS-PML provides high absorption at large angles. In Fig. 4, we show the angular reflection spectra of NS-PML with different numbers of layers, $L = 8$, 16, 32, 64. The more layers, the higher the absorption (doubling L reduces reflection by about 30 dB). When $\theta > 60°$, the reflection exponentially increases.

VI. CONCLUSION

We developed a nonstandard (NS) finite difference time domain (NS-FDTD) algorithm for the conductive Maxwell's equations and a NS-version of the perfectly matched layer (NS-PML). Heretofore, the NS-FDTD algorithm has performed successfully in many nanoscale simulations [3, 4]. However, it is sometimes unstable after a large number of wave periods (for example, in whispering gallery mode calculations) due to corner reflections, but the NS-PML ensures absolute stability. We showed that the NS-PML provides more effective absorption than conventional NS-Mur and NS-Higdon absorbing boundary conditions.

Comparing the NS-PML with the conventional or standard (S) PML, the absorption performance is the same because it is determined by the given splitted conductivities. But although the memory cost is the same, the NS stability is better than the S one (the NS computational wave velocity can be increased by: 10% in 2-D; 35% in 3-D) [3].

The "unsplit" PML has been proposed [13, 14]. Since the unsplit PML has lower computational cost, in future work we will try to develop a NS-version of the unsplit PML.

APPENDIX A
NONSTANDARD FINITE DIFFERENCE MODEL

A high accuracy spatial finite difference model is found by optimizing to monochromatic wave propagation [2]. In one-dimension, the conventional central finite difference (FD) approximation is defined by

$$\partial_x \psi(x,t) \cong \frac{d_x \psi(x,t)}{h}, \tag{36}$$

where $d_x \psi(x,t) = \psi(x + h/2, t) - \psi(x - h/2, t)$. For monochromatic waves $\psi_0 = e^{i(kx \pm \omega t)}$, we have an exact nonstandard (NS) FD expression,

$$\frac{d_x \psi_0}{s(k,h)} = \partial_x \psi_0, \quad s(k,h) = \frac{2}{k} \sin\left(\frac{kh}{2}\right). \tag{37}$$

The exact NS-FD expression of (37) cannot be generalized beyond one dimension, but it is possible to

construct a high accuracy NS-FD expression with respect to plane waves of the form,

$$\nabla^2\psi_0(\mathbf{r},t) \cong \frac{\mathbf{d}_0^2\psi_0(\mathbf{r},t)}{s(k,h)^2}, \tag{38}$$

where

$$\begin{aligned}\mathbf{d}_0^2 = \mathbf{d}^2 &+ \gamma_1\left(d_x^2d_y^2 + d_y^2d_z^2 + d_z^2d_x^2\right)\\ &+ \gamma_2 d_x^2d_y^2d_z^2,\end{aligned} \tag{39}$$

where $\mathbf{d} = (d_x, d_y, d_z)$ and

$$\gamma_1 \cong \frac{1}{6} + \frac{k^2h^2}{180} - \frac{k^4h^4}{23040} + \cdots, \tag{40}$$

$$\gamma_2 \cong \frac{1}{30} + \frac{k^2h^2}{360} - \frac{k^4h^4}{7200} + \cdots. \tag{41}$$

Details of this derivation are given in [2, 3]. The error of the NS-FD approximation is

$$\frac{1}{\psi_0}\left(\nabla^2 - \frac{\mathbf{d}_0^2}{s(k,h)^2}\right)\psi_0 \cong \frac{(kh)^6k^2}{20160} + \cdots. \tag{42}$$

Since the error of the conventional FD approximation is

$$\frac{1}{\psi_0}\left(\nabla^2 - \frac{\mathbf{d}^2}{h^2}\right)\psi_0 \cong \frac{(kh)^2k^2}{12} + \cdots, \tag{43}$$

(38) is almost exact.

We need to approximate $\nabla\times$ in Maxwell's equations, but $\mathbf{d}_0 = (d_x^0, d_y^0, d_z^0)$ which satisfies $\mathbf{d}_0^2 = \mathbf{d}_0 \cdot \mathbf{d}_0$ does not exist. Instead, we require that

$$\mathbf{d}_0^2 = \mathbf{d}_0 \cdot \mathbf{d} = \mathbf{d} \cdot \mathbf{d}_0, \tag{44}$$

and find that

$$\mathbf{d}_0 = \begin{bmatrix} d_x\left(1 + \frac{\gamma_1}{2}\left(d_y^2 + d_z^2\right) + \frac{\gamma_2}{3}d_y^2d_z^2\right)\\ d_y\left(1 + \frac{\gamma_1}{2}\left(d_x^2 + d_z^2\right) + \frac{\gamma_2}{3}d_x^2d_z^2\right)\\ d_z\left(1 + \frac{\gamma_1}{2}\left(d_x^2 + d_y^2\right) + \frac{\gamma_2}{3}d_x^2d_y^2\right)\end{bmatrix}. \tag{45}$$

APPENDIX B
EIGENVALUE AND STABILITY

An algorithm is given by

$$\mathbf{\Psi}^n = A^n\mathbf{\Psi}^0, \tag{46}$$

where $t = n\Delta t$ ($n =$ integer), $\mathbf{\Psi}(\mathbf{r},t) \to \mathbf{\Psi}^n$, and

$$A = \begin{pmatrix} 0 & 1\\ -c_1 & 2c_2\end{pmatrix}. \tag{47}$$

If $|A| \neq 0$ such as (33), A is diagonalizable and the algorithm stability is given by $|\lambda| \leq 1$ ($\lambda =$ eigenvalue of A) [15]. λ is found by solving

$$|A - \lambda I| = 0, \tag{48}$$

where I is the identity matrix. We obtain

$$\lambda = c_2 \pm \sqrt{c_2^2 - c_1}. \tag{49}$$

Using $|\lambda| \leq 1$, the algorithm stability becomes

$$c_2^2 \leq c_1 \leq 1. \tag{50}$$

REFERENCES

[1] R. E. Mickens, "Nonstandard Finite Difference Models of Differential Equations," *World Scientific*, 1994.

[2] J. B. Cole, "High-Accuracy Yee Algorithm Based on Nonstandard Finite Differences: New Developments and Verifications," *IEEE Trans. Antennas Propag.*, vol. 50, no. 9, pp. 1185-1191, 2002.

[3] J. B. Cole, S. Banerjee, and M. I. Haftel, "High Accuracy Nonstandard Finite Difference Time-Domain Algorithms for Computational Electromagnetics: Applications to Optics and Photonics," chap. 4, pp. 89-109 in Advances in the Applications of Nonstandard Finite Difference Schemes, R. E. Mickens, ed., *Scientific*, 2005.

[4] N. Okada and J. B. Cole, "Simulation of Whispering Gallery Modes in the Mie Regime using the Nonstandard Finite-Difference Time Domain Algorithm," *J. Opt. Soc. Am. B*, vol. 27, no. 4, pp. 631-639, 2010.

[5] J. B. Cole and D. Zhu, "Improved Version of the Second-Order Mur Absorbing Boundary Condition Based on a Nonstandard Finite Difference Model," *Applied Computational Electromagnetic Society (ACES) Journal*, vol. 24, no. 4, pp. 375-381, 2009.

[6] M. F. Hadi, "Wide-Angle Absorbing Boundary Conditions for Low and High-Order FDTD Algorithms," *Applied Computational Electromagnetic Society (ACES) Journal*, vol. 24, no. 1, pp. 9-15, 2009.

[7] J. P. Berenger, "A Perfectly Matched Layer for the Absorption of Electromagnetic Waves," *J. Comput. Phys.*, vol. 114, no. 2, pp. 185-200, 1994.

[8] W. C. Chew and J. M. Jin, "Perfectly Matched Layers in the Discretized Space: An Analysis

and Optimization," *Electromagnetics*, vol. 16, pp. 325-340, 1996.

[9] Z. Wu and J. Fang, "Numerical Implementation and Performance of Perfectly Matched Layer Boundary Condition for Waveguide Structures," *IEEE Trans. Microwave Theory Tech.*, vol. 43, no. 12, pp. 2676-263, 1995.

[10] S. Abarbanel and D. Gottlieb, "A Mathematical Analysis of the PML Method," *J. Comput. Phys.*, vol. 134, no. 2, pp. 357-363, 1997.

[11] F. L. Teixeira and W. C. Chew, "Finite-Difference Computation of Transient Electromagnetic Waves for Cylindrical Geometries in Complex Media," *IEEE Trans. Geosci. Remote Sens.*, vol. 38, no. 4, pp. 1530-1543, 2000.

[12] R. L. Higdon, "Absorbing Boundary Conditions for Difference Approximations to the Multi-Dimensional Wave Equation," *Mathematics of Computation*, vol. 47, no. 176, pp. 437-459, 1986.

[13] W. C. Chew and W. H. Weedon, "A 3D Perfectly Matched Medium from Modified Maxwell's Equations with Stretched Coordinates," *Microwave Optical Tech. Lett.*, vol. 7, no. 13, pp. 599-604, 1994.

[14] L. Zhao and A. C. Cangellaris, "A General Approach for the Development of Unsplit-Field Time-Domain Implementations of Perfectly Matched Layers for FDTD Grid Truncation," *IEEE Microwave and Guided Wave Letters*, vol. 6, no. 5, pp. 209-211, 1996.

[15] S. Wang and F. L. Teixeira, "Some Remarks on the Stability of Time-Domain Electromagnetic Simulations," *IEEE Trans. Antennas Propag.*, vol. 52, no. 3, pp. 895-898, 2004.

Naoki Okada is a Ph.D. student in the Graduate School of Systems and Information Engineering, University of Tsukuba, Japan. His main research interests are in computational optics, electromagnetic simulations, and algorithm development. In particular, he focuses on the use of high accuracy nonstandard finite difference time domain (FDTD) algorithms for light scattering simulation and optical waveguide device design. He is also interested in parallel computation using the graphics processing unit (GPU), and photorealistic rendering of structural colors such as Morpho butterfly. Please visit his web page at http://nsfdtd.org/.

James B. Cole graduated from the University of Maryland (USA) with a Ph.D. in Particle Physics. During post-doctorate research at the NASA Goddard Space Flight Center, he began his career in numerical simulations (cosmic ray antiproton flux). Later, he worked on stochastic simulations at the Army Research Laboratory, and visited the NTT Basic Research Laboratory (Japan) for one year. As a research physicist at the Naval Research Laboratory, working on the Connection Machine, he developed the earliest nonstandard finite difference (NS-FD) models for acoustic simulations. After joining the faculty of the University of Tsukuba (Japan), where he is a professor, he extended NS-FD models to computational electromagnetics and optics.